1999ASPC..184....3C

*3rd Advances in Solar Physics Euroconference:*
*Magnetic Fields and Oscillations*
*ASP Conference Series, Vol. 184, 1999*
*B. Schmieder, A. Hofmann, J. Staude, eds.*

# High Resolution Spectropolarimetry and Magnetography

Manuel Collados
*Instituto de Astrofísica de Canarias, E-38200 La Laguna, Tenerife, Spain*

**Abstract.** From an observational point of view, magnetic field leaves its imprint, via Zeeman effect, on spectral line splitting and the induced wavelength dependence of the polarization state of the observed photons. The characteristics of the most recent polarimetric analyzers are described, together with their limitations. Next, inversion techniques are presented as the most accurate diagnostic tools available at present to determine the properties of magnetic field, derived from its polarization signature. Finally, the importance of feeding inversion codes with the adequate physics are stressed.

## 1. Introduction

Magnetism plays a crucial role in our understanding of the Sun. Nevertheless the physics behind the numerous solar magnetic phenomena is still far from giving us the answer to old questions, despite the advances in theory, numerical simulations, technical development, and quality of observational data. For instance, the properties of magnetic flux as it emerges or disappears on the solar surface are not established yet. Convective collapse was suggested a long time ago (Parker 1978) as the process to create the strong magnetic fields observed in faculae and photospheric network. Nonetheless, definite observational evidences that this process takes place are still lacking. Numerical calculations are nowadays beginning to be able to simulate the structure of isolated flux-tubes and their interaction with the surrounding convection (see, e.g. Steiner et al. 1998), but it is not clear enough how well they fit to observed data. Spot structure, with its intricate penumbral structure, is the subject of accurate studies with sophisticated analysis techniques (e.g., Martínez Pillet 1997, and references therein). Chromospheric heating and its relationship with magnetic fields represents one of the most difficult and interesting topics. Many other examples might be quoted, all of them sharing magnetic field as a principal constituent.

The analysis of magnetic field properties is carried out in three steps. Firstly, accurate and complete polarimetric data have to be obtained. Secondly, this signature has to be converted into a magnetic signal, via more or less sophisticated inversion codes, which invariably use prescribed physical models. Finally, since various approaches may give similar results in what concerns the quality of the fits to line profiles, the adequacy of the retrieved models can only be determined by their ability in reproducing observations other than those



© Astronomical Society of the Pacific • Provided by the NASA Astrophysics Data System

1999ASPC..184....3C



strictly used to obtain the free parameters of the models. All these points are addressed in the following.

## 2. Polarization Analysis

The analysis of the polarization state of the light is carried out by modulating the intensity transmitted by an optical system. This is achieved by a combination of one or more retarders followed by a polarizer or a polarizing beamsplitter. By changing the retardance, or the relative orientation between the components, a number of intensity measurements $N_i$ $(i = 1, \ldots, n)$ are obtained which are linear combinations (modulation scheme) of the input Stokes parameters $I$, $Q$, $U$, and $V$ characterizing the light under analysis.

In vectorial form, this may be written as

$$\vec{N} = \mathbf{M}\vec{I}, \tag{1}$$

where $\vec{N} = (N_1, N_2, \ldots, N_n)^\dagger$ is a vector containing $n$ intensity measurements, $\vec{I} = (I, Q, U, V)^\dagger$ is the input Stokes vector, $\mathbf{M}$ is the coefficient matrix (usually referred to as modulation matrix), and the symbol $\dagger$ represents matrix transposition.

A modulation efficiency may be defined to characterize the ability of a given modulation scheme to recover the input Stokes vector. Before writing that definition, some interesting polarization properties are presented:

1. The intensity transmitted by an optical system formed by an ideal retarder and an ideal linear polarizer is

$$I_{\text{trans}} = (I + \alpha Q + \beta U + \gamma V). \tag{2}$$

In this equation, and in the following, the transmission 1/2 of the linear polarizer has been thrown away, since it is only a constant factor that does not affect the modulation. The coefficients multiplying $Q$, $U$, and $V$ fulfill

$$\alpha^2 + \beta^2 + \gamma^2 = 1. \tag{3}$$

This statement is readily proven after the Mueller matrices of an ideal polarizer and retarder, which give

$$\begin{aligned} \alpha &= \cos^2 2\theta + \sin^2 2\theta \cdot \cos\delta, \\ \beta &= \sin 2\theta \cdot \cos 2\theta\,(1 - \cos\delta), \\ \gamma &= -\sin 2\theta \cdot \sin\delta. \end{aligned} \tag{4}$$

$\theta$ is the angle formed by the directions of the fast axis of the retarder and the transmitting axis of the polarizer, and $\delta$ is the retardance of the retarder.

© Astronomical Society of the Pacific • Provided by the NASA Astrophysics Data System

1999ASPC..184....3C



2. The intensity transmitted by an optical system formed by two ideal retarders and an ideal linear polarizer has the same dependence on $I$, $Q$, $U$, and $V$ as in Eq. 2, the coefficients also related by Eq. 3 (but with dependences different than those shown in Eqs. 4).

   This identity is immediately obtained after the corresponding Mueller matrices. It is always possible to find a single equivalent ideal retarder with the same $\alpha$, $\beta$, and $\gamma$ coefficients.

3. Any optical system formed by an arbitrary number of ideal retarders and an ideal linear polarizer can be substituted by a single equivalent ideal retarder and a polarizer which give the same transmitted intensity.

   This statement follows directly from item 2, just by merging first the two retarders nearest the polarizer into a single one. Next, this would be combined with the third one, and so on. At the end, a single equivalent retarder would remain.

Accordingly, a modulation system may be considered as a set of $n$ retarders, each one followed by a polarizer, to give a set of different transmitted intensities $N_i$ ($i = 1, \ldots, n$), related to the input $\vec{I}$ by Eq. 1. If the system of equations is squared (i.e., $n = 4$) and all the combinations are linearly independent, the inverse matrix ($\mathbf{D} = \mathbf{M}^{-1}$, demodulation matrix) exists, and the input Stokes vector can be recovered from the measured intensities according to

$$\vec{I} = \mathbf{D}\vec{N}, \tag{5}$$

If the number of measurements is larger than 4, but with the rank of $\mathbf{M}$ being 4, it is always possible to find at least one matrix $\mathbf{D}$ such that $\mathbf{DM} = \mathbf{1}$, where $\mathbf{1}$ is the $4 \times 4$ identity matrix. From all the possible $\mathbf{D}$ matrices, the Singular Value Decomposition (SVD) method (Press et al. 1986) allows to obtain the "best" one in a least squares sense (minimizing the sum of the squared coefficients of $\mathbf{D}$). This property will be useful later in the definition of the most efficient modulation schemes.

For ideal retarders and polarizers, the coefficients of the modulation matrix $\mathbf{M}$ are such that

$$\sum_{j=2}^{4} M_{ij}^2 = 1, \tag{6}$$

with

$$M_{i1} = 1, \qquad i = 1, \cdots, n. \tag{7}$$

Now, we are in the position to define the efficiency of a modulation scheme as a four-element vector $\vec{\varepsilon}$ whose components are

$$\varepsilon_i = \left( n \sum_{j=1}^{n} D_{ij}^2 \right)^{-1/2}. \tag{8}$$

This definition was first introduced by Sánchez Almeida et al. (1994).

© Astronomical Society of the Pacific • Provided by the NASA Astrophysics Data System

1999ASPC..184....3C



The physical interpretation of Eq. 8 is straightforward. Assuming that all the measured intensities have the same uncertainty $\sigma$ (due, for instance, to photon noise), error propagation in Eq. 5 gives

$$\sigma_i^2 = \sigma^2 \sum_{j=1}^{n} D_{ij}^2, \tag{9}$$

where $\sigma_i$ $(i = 1, 2, 3, 4)$ represents the uncertainty in the derived Stokes parameters.

Thus, in order to minimize $\sigma_i$ (and, as a consequence, maximize the signal to noise ratio in every Stokes parameter), it is advisable to use a modulation scheme which minimizes the sum of the squared coefficients of the demodulation matrix. It is now clear why, when $n > 4$, the use of SVD is adequate to obtain the optimum demodulation matrix $\mathbf{D}$ from $\mathbf{M}$. However, Eq. 9 does not allow to compare modulation schemes with a different number $n$ of intensity measurements (in principle, it is expected that, for equal efficiency, modulation schemes with a larger value of $n$ will lead to lower $\sigma_i$'s). The contribution to the variance by a single measurement (normalized variance) will be $n$ times larger than $\sigma_i$, i.e.,

$$\bar{\sigma}_i^2 = n\sigma^2 \sum_{j=1}^{n} D_{ij}^2 = \frac{\sigma^2}{\varepsilon_i^2}, \tag{10}$$

where $\bar{\sigma}$ indicates normalized variance.

For a given optical setup, detector, integration time and the same remaining parameters, $\sigma$ is constant. Thus, the larger the efficiency $\varepsilon_i$, the less noisy the corresponding Stokes parameter.

Now it can be proved that for a modulation scheme based upon a set of ideal retarders and an ideal linear polarizer

$$\varepsilon_1 \leq 1, \tag{11}$$

$$\sum_{i=2}^{4} \varepsilon_i^2 \leq 1. \tag{12}$$

Inequality 11 follows directly from the fact that $\mathbf{DM} = \mathbf{1}$, from which

$$\sum_{j=1}^{n} D_{1j} M_{j1} = 1. \tag{13}$$

To show it, let $S_1$ be

$$S_1 = \sum_{j=1}^{n} D_{1j}^2 = \frac{1}{n\varepsilon_1^2}. \tag{14}$$

The maximum value of $\varepsilon_1$ is obtained when $S_1$ is a minimum. After Eqs. 13 and 14

© Astronomical Society of the Pacific • Provided by the NASA Astrophysics Data System

1999ASPC..184....3C



$$\frac{\partial \varepsilon_1}{\partial D_{1j}} = 0 \Rightarrow \frac{\partial S_1}{\partial D_{1j}} = 0 \Rightarrow D_{1j} = \frac{M_{j1}}{M_{n1}} D_{1n}, \qquad (j = 1, \ldots, n). \tag{15}$$

Introducing this result into Eq. 13, one obtains

$$\sum_{j=1}^{n} M_{j1}^2 = \frac{M_{n1}}{D_{1n}}. \tag{16}$$

Combining Eqs. 7, 14, 15, and 16, the minimum value of $S_1$ ($S_1^{\min}$) can be written as

$$S_1 \geq S_1^{\min} = 1/\sum_{j=1}^{n} M_{j1}^2 = \frac{1}{n}. \tag{17}$$

Introducing Eq. 17 into Eq. 14, inequality 11 is reached.

The demonstration of inequality 12 is similar, but now using Eq. 6 and

$$\sum_{j=1}^{n} D_{ij} M_{ji} = 1, \qquad (i = 2, 3, 4). \tag{18}$$

Now the maximum value of $\sum_{i=2}^{4} \varepsilon_i^2$ turns out to be

$$(\sum_{i=2}^{4} \varepsilon_i^2)^{\max} = \frac{1}{n} \sum_{j=1}^{n} \sum_{i=2}^{4} M_{ji}^2, \tag{19}$$

which, by virtue of Eq. 6, gives inequality 12. It can be readily found, by evaluating the second derivatives, that the thresholds obtained are maximum efficiencies. Thus, the larger the efficiency (as defined by Eq. 8), the larger the S/N ratio of the recovered Stokes parameters.

## 2.1. Temporal and spatial modulation

In solar observations, much care must be taken when measuring polarization signals with high accuracy because of two main effects:

- Gain-table uncertainties:

  This problem appears when polarizing beamsplitters are used, together with the adequate retarders, to measure different linear combinations of the Stokes parameters with different detectors at the same time (or different pixels of a two-dimensional sensor). The limitations of this kind of measurements has been reported by many authors (e.g. Stenflo & Povel 1985, Sánchez Almeida & Martínez Pillet 1994, Keller et al. 1994).

  A simple example may illustrate this case. Assume that $I \pm V$ are measured, using a perfect quarter-wave plate and an ideal, correctly aligned, polarizing beamsplitter. The measured intensity of the two outcoming beams ($I^+$ and $I^-$) will be

© Astronomical Society of the Pacific • Provided by the NASA Astrophysics Data System

1999ASPC..184....3C



$$I^+ = K(I+V), \quad (20)$$
$$I^- = (K+\delta K)(I-V), \quad (21)$$

where $\delta K$ is the uncertainty in the gain-table determination after a flat-fielding procedure. Often $\delta K/K$ is usually of the order of $10^{-2}$. Adding and subtracting both beams to get the measured total ($I_{\rm meas}$) and circular polarization ($V_{\rm meas}$) intensities, one gets

$$I_{\rm meas} = I^+ + I^- = 2K \cdot I + \delta K \cdot (I-V), \quad (22)$$
$$V_{\rm meas} = I^+ - I^- = 2K \cdot V - \delta K \cdot (I-V). \quad (23)$$

As the degree of circular polarization ($V/I$) observed in many solar magnetic phenomena is of the order of $10^{-1}$, the maximum order of magnitude of the different terms in the last two equations can be estimated to be

$$\frac{\delta K \cdot (I-V)}{2K \cdot I} \sim 10^{-2}, \quad (24)$$
$$\frac{\delta K \cdot (I-V)}{2K \cdot V} \sim 10^{-1}. \quad (25)$$

Thus, $I_{\rm meas}$ and $V_{\rm meas}$ are no longer proportional to $I$ and $V$, but are contaminated by additional terms introduced by gain-table uncertainties. The cross-talk term $I \rightarrow V$ is especially important. Note that even the degree of circular polarization can not be recovered.

Simple order of magnitude calculations may be done taking into account the four Stokes parameters, with the result that the $I \rightarrow Q, U, V$ crosstalk is crucial for an accurate determination of the Stokes parameters of the incoming light. For large two-dimensional detectors, measuring the Stokes parameters at different points and/or wavelengths, the gain-table uncertainty may be kept statistically (very near) zero, but variations from pixel to pixel can not be avoided.

- Seeing-induced crosstalk:

The above described contamination can be reduced if a single detector is used to register different linear combinations of the input Stokes parameter, so that the gain-factor can be kept constant. To that aim, some temporally varying polarizing optical element is introduced in the beam (e.g, Stenflo & Povel 1985, Elmore et al. 1992, Martínez Pillet et al. 1999). Now the problem comes from the rapidly varying conditions in the turbulent Earth's atmosphere, causing variations in transparency, image motion and blurring. With a single beam system, this limitation may be overcome with very large modulation frequencies ($> 1$ kHz). This is the case of the system proposed by Stenflo & Povel (1985).

© Astronomical Society of the Pacific • Provided by the NASA Astrophysics Data System

1999ASPC..184....3C



Using again a simple circular polarization example, assume that two measurements are obtained at two instants, $t_1$ and $t_2$, giving rise to the detected $I(t_1)$ and $I(t_2)$. Ideally one would want these two measurements to be proportional to $I \pm V$. If the two measurements are not taken fast enough to freeze the Earth's atmosphere, one would have

$$I(t_1) = K(I+V), \tag{26}$$
$$I(t_2) = K[(I+\delta I)-(V+\delta V)], \tag{27}$$

where $\delta I$ and $\delta V$ represent the changes in the input Stokes parameters because the observed region may not be exactly the same, and may be estimated to be of the order of $\delta I/I \sim \delta V/V \sim 10^{-2}$. Adding and subtracting $I(t_1)$ and $I(t_2)$ to get $I_{\rm meas}$ and $V_{\rm meas}$ yields

$$I_{\rm meas} = I(t_1)+I(t_2) = 2K\cdot I + K\cdot(\delta I - \delta V), \tag{28}$$
$$V_{\rm meas} = I(t_1)-I(t_2) = 2K\cdot V - K\cdot(\delta I - \delta V). \tag{29}$$

The order of magnitude of the different terms in the right-hand side of the last two equations is

$$\frac{K\cdot(\delta I-\delta V)}{2K\cdot I} \sim 10^{-2}, \tag{30}$$
$$\frac{K\cdot(\delta I-\delta V)}{2K\cdot V} \sim 10^{-1}. \tag{31}$$

Again temporal modulation is not able to recover the input Stokes parameters if not carried out with samplings much smaller that the typical time needed for the conditions of the Earth's atmosphere to change.

An often used solution (Elmore et al. 1992, Martínez Pillet et al 1999) comes from a mixed procedure, using spatial modulation (to avoid seeing-induced crosstalk) and temporal modulation (to avoid gain-table uncertainties). In a simple case as those described above, one would have now four measurements (two at instant $t_1$ from the two beams generated by a polarizing beamsplitter, and another two at instant $t_2$):

$$I^+(t_1) = K(I+V), \tag{32}$$
$$I^-(t_1) = (K+\delta K)(I-V), \tag{33}$$
$$I^+(t_2) = K[(I+\delta I)-(V+\delta V)], \tag{34}$$
$$I^-(t_2) = (K+\delta K)[(I+\delta I)+(V+\delta V)]. \tag{35}$$

Combining $I^+(t_1)$ and $I^+(t_2)$, one gets Eqs. 28 and 29, giving rise to $I^+_{\rm meas}$ and $V^+_{\rm meas}$. Similar equations are obtained from Eqs. 33 and 35 to give $I^-_{\rm meas}$ and $V^-_{\rm meas}$. Averaging both beams yields

© Astronomical Society of the Pacific • Provided by the NASA Astrophysics Data System

1999ASPC..184....3C



$$I_{\rm meas} = \frac{1}{2}(I^+_{\rm meas} + I^-_{\rm meas}) = (2K + \delta K)(I + \frac{1}{2}\delta I + \frac{1}{2}\delta V), \quad (36)$$

$$V_{\rm meas} = \frac{1}{2}(V^+_{\rm meas} + V^-_{\rm meas}) = (2K + \delta K)(V + \frac{1}{2}\delta V) + \frac{1}{2}\delta K \cdot \delta I. \quad (37)$$

Now the last term in the right-hand side of the last equation is of order of $\delta K \cdot \delta I / K \cdot V \sim 10^{-3}$ and can be neglected in most occasions. The term in $\delta V$ in Eq. 36 can also be usually thrown away as $\delta V / I \sim 10^{-3}$. It turns out that with this procedure the degree of circular polarization can be accurately obtained

$$\frac{V_{\rm meas}}{I_{\rm meas}} = \frac{V + \frac{1}{2}\delta V}{I + \frac{1}{2}\delta I}, \quad (38)$$

regardless of the gain-table uncertainties and seeing-induced crosstalk, if these effects can be kept of second order magnitude. This implies that correlation techniques must be carried out to stabilize the image. Present on-line tracking techniques can reduce image motion down to a value of the order of 0.01 arcsec (Ballesteros et al. 1996). Image blurring is more difficult to handle because of the lack of operating adaptive optics at present solar telescopes.

Simultaneous temporal and spatial modulation has the additional advantage that the S/N ratio can be improved by simply increasing the exposure time of the individual measurements $N_i$, or cycling them and adding on real time all those images corresponding to the same state of the retarders. Both solutions result in a larger effective integration time, although the latter solution is to be preferred to minimize seeing-induced crosstalk.

## 2.2. Wavelength Dependence of the Polarization Signal

Apart from the measurement itself, there are several factors which directly affect the quality of the polarimetric data obtained. These are the instrumental polarization, atmospheric seeing and the amplitude of the observed polarization signal. Their influence and wavelength dependence is commented below.

In general, solar telescopes have not been designed for accurate polarimetric studies and the light is usually reflected several times by mirrors in the optical path before the polarimetric analysis is done (except for the French-Italian telescope THEMIS, which is expected to give regular data of unprecedent polarization quality in the near future). A reflection on a mirror alters the polarization state of light and, for this reason, an accurate telescope calibration is required. To that aim, geometrical models of telescopes are constructed (e.g., Balasubramaniam et al. 1985, Capitani et al. 1989) depending on the refractive indices of the mirrors. At optical wavelengths, these indices are usually evaluated using large polarizing sheets located in front of the telescope. In the near-infrared it is more difficult to get those large polarizing sheets. Fortunately, the instrumental polarization induced by reflections is less severe in this wavelength region. The left plot in Fig. 1 shows the wavelength variation of the refractive index of aluminium (real and imaginary parts) taken from Lide (1993), giving rise to the variation of the retardance induced by a reflection on an aluminized mirror with the incident angle at 500 nm and 1.56 $\mu$m shown in the right panel of Fig. 1.

© Astronomical Society of the Pacific • Provided by the NASA Astrophysics Data System

1999ASPC..184....3C



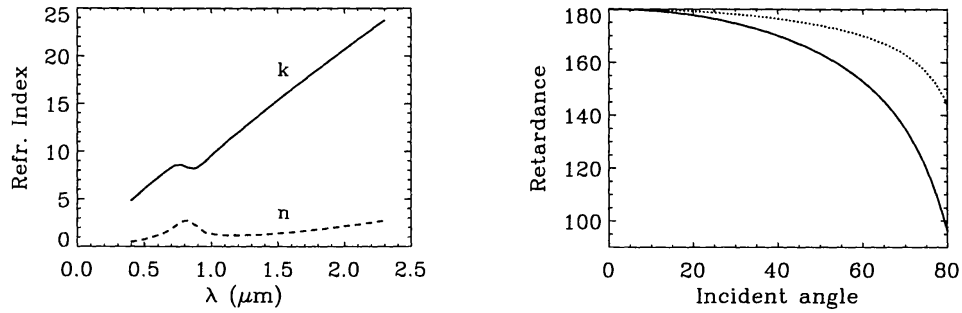


Figure 1. **Left**: Variation with wavelength of the complex refractive index of aluminium ($n + ik$). **Right**: Variation of the retardance introduced by an aluminized mirror with the incident angle at 500 nm (solid line) and 1.56 $\mu$m (dashed line)

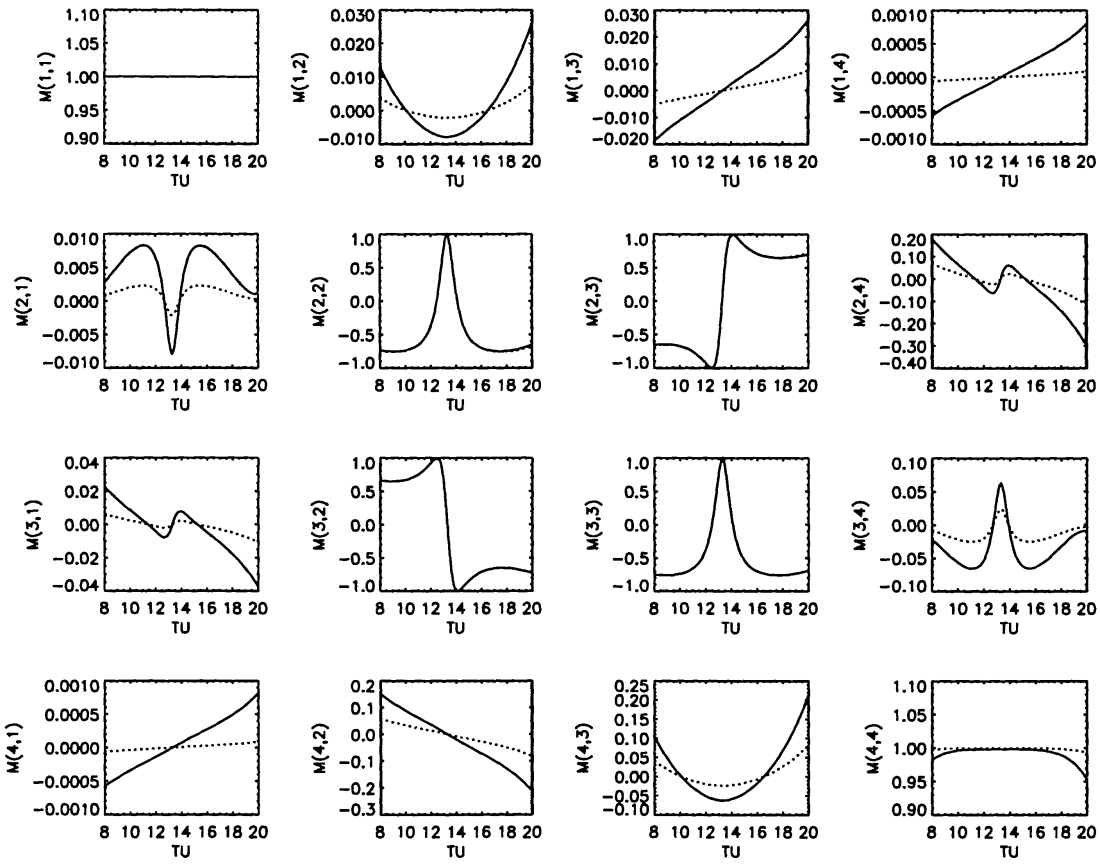


Figure 2. Daily variation of the coefficients of the Mueller matrix corresponding to the German VTT at Observatorio del Teide (Tenerife), at two wavelengths: 500 nm (solid line) and 1.56 $\mu$m (dotted line) on July 1$^{st}$.

© Astronomical Society of the Pacific • Provided by the NASA Astrophysics Data System

1999ASPC..184....3C



As an example of the wavelength dependence of the instrumental polarization induced by a telescope, Fig. 2 shows the daily variation of the Mueller matrix of the German VTT at Observatorio del Teide (Tenerife, Canary Islands) at 500 nm and 1.56 $\mu$m. As can be seen, the cross-talk terms and their daily variations are much less dramatic in the near-infrared than in optical wavelengths.

In addition, the influence of the Earth's atmosphere is significantly smaller in the near infrared. The Fried's parameter, $r_o$, (which indicates the maximum size of a telescope not affected by seeing) varies as $\lambda^{6/5}$ (Fried 1965). A value of $r_o$ of 12cm at 500 nm is equivalent to $r_o = 48$ cm at 1.6 $\mu$m, close to the diameter of most of the ground-based solar telescopes. Thus, while visible images would be clearly affected by seeing, the spatial resolution in the near infrared might be mainly limited by the optical system used. Although the theoretical resolution of the telescopes at these wavelengths is lower, it is still good enough to make high angular resolution observations possible. For instance, at the VTT of the Observatorio del Teide (with a diameter of 70cm), the theoretical resolution is 0.58 arcsec at 1.6 $\mu$m,

On the other hand, the Zeeman splitting is considerably larger in the near infrared. While the width of spectral lines increases proportionally to $\lambda$, the magnetic splitting does as $\lambda^2$. The net effect is that lines at 1.6 $\mu$m are more sensitive to magnetic fields than at 500 nm, for equal Landé factor. In other words, for observations with the same signal-to-noise ratio, the near infrared allows the detection of smaller fields (note that the amplitude of the polarization signal is proportional to the magnetic splitting in the weak field regime).

## 3. Examples of modulation schemes

In the following, three full polarimetric systems operating with different devices are compared.

### 3.1. ZIMPOL

Stenflo et al. (1992) suggested a scheme for ZIMPOL II based on two piezoelastic modulators and a linear polarizer, with a theoretical modulation matrix given by

$$\mathbf{M} = \begin{pmatrix} 1 & 0.67 & -0.66 & 0.26 \\ 1 & -0.29 & 0 & -0.40 \\ 1 & 0.11 & 0.66 & 0.26 \\ 1 & -0.49 & 0 & 0.92 \end{pmatrix}, \tag{39}$$

from where the efficiency turns out to be

$$\vec{\varepsilon} = (0.87, 0.39, 0.42, 0.46) \tag{40}$$

with a total polarization efficiency

$$\sqrt{\varepsilon_2^2 + \varepsilon_3^2 + \varepsilon_4^2} = 0.73. \tag{41}$$

© Astronomical Society of the Pacific • Provided by the NASA Astrophysics Data System

1999ASPC..184....3C



### 3.2. ASP

The Advanced Stokes Polarimeter (Elmore et al. 1992), operating at Sacramento Peak Observatory, uses a rotating waveplate ($\delta = 107°$ at 630 nm) and a linear polarizer to modulate the outcoming intensity. The theoretical modulation matrix of the ASP at 630 nm is

$$\mathbf{M} = \begin{pmatrix} 1 & 0.77 & 0.41 & -0.36 \\ 1 & -0.06 & 0.41 & -0.86 \\ 1 & -0.06 & -0.41 & -0.86 \\ 1 & 0.77 & -0.41 & -0.36 \\ 1 & 0.77 & 0.41 & 0.36 \\ 1 & -0.06 & 0.41 & 0.86 \\ 1 & -0.06 & -0.41 & 0.86 \\ 1 & 0.77 & -0.41 & 0.36 \end{pmatrix}, \tag{42}$$

from where the efficiency is

$$\vec{\varepsilon} = (0.76, 0.41, 0.41, 0.66), \tag{43}$$

with a total polarization efficiency

$$\sqrt{\varepsilon_2^2 + \varepsilon_3^2 + \varepsilon_4^2} = 0.88. \tag{44}$$

For a modulation scheme like this one, based on a rotating waveplate, the maximum efficiency is obtained with a retardance $\delta = 130.4°$, in which case,

$$\vec{\varepsilon} = (0.95, 0.52, 0.52, 0.52) \tag{45}$$

with a total polarization efficiency

$$\sqrt{\varepsilon_2^2 + \varepsilon_3^2 + \varepsilon_4^2} = 0.91 \tag{46}$$

### 3.3. TIP and LPSP

Recently the IAC built two ASP-like polarimeters, TIP (Tenerife Infrared Polarimeter) for the wavelength range 1-2.3 $\mu$m, and LPSP (La Palma Stokes Polarimeter) for the range 450-700 nm. Instead of using a rotating waveplate, TIP and LPSP have two ferroelectric liquid crystals (FLCs). These devices are retarders whose fast axis can be switched between two positions depending on the value of an externally applied voltage. The FLCs and a polarizing beamsplitter are located after the spectrograph entrance slit. For further details, see Martínez Pillet et al. (1999). The experimental modulation matrix obtained with TIP at the German VTT operating at the Observatorio del Teide is

$$\mathbf{M} = \begin{pmatrix} 1.00 & 0.47 & -0.68 & 0.48 \\ 1.00 & -0.91 & -0.19 & -0.13 \\ 1.00 & -0.11 & 0.57 & 0.72 \\ 1.00 & 0.68 & 0.27 & -0.58 \end{pmatrix}, \tag{47}$$

from which

© Astronomical Society of the Pacific • Provided by the NASA Astrophysics Data System

1999ASPC..184....3C



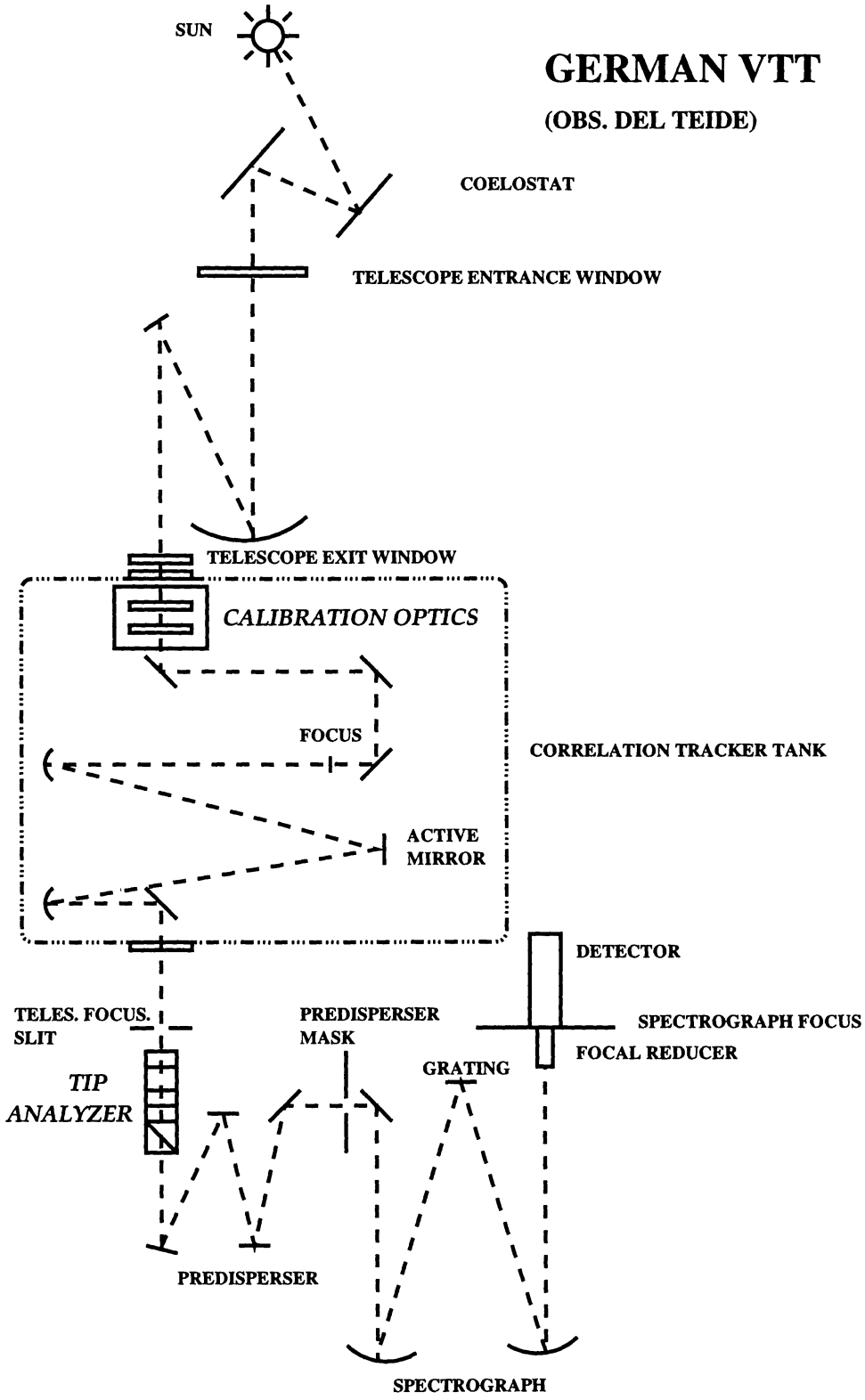


Figure 3. Sketch of the German VTT at Observatorio del Teide (Tenerife) showing the locations of the near infrared polarimetric analyzer (TIP) and the calibration optics

© Astronomical Society of the Pacific • Provided by the NASA Astrophysics Data System

1999ASPC..184....3C



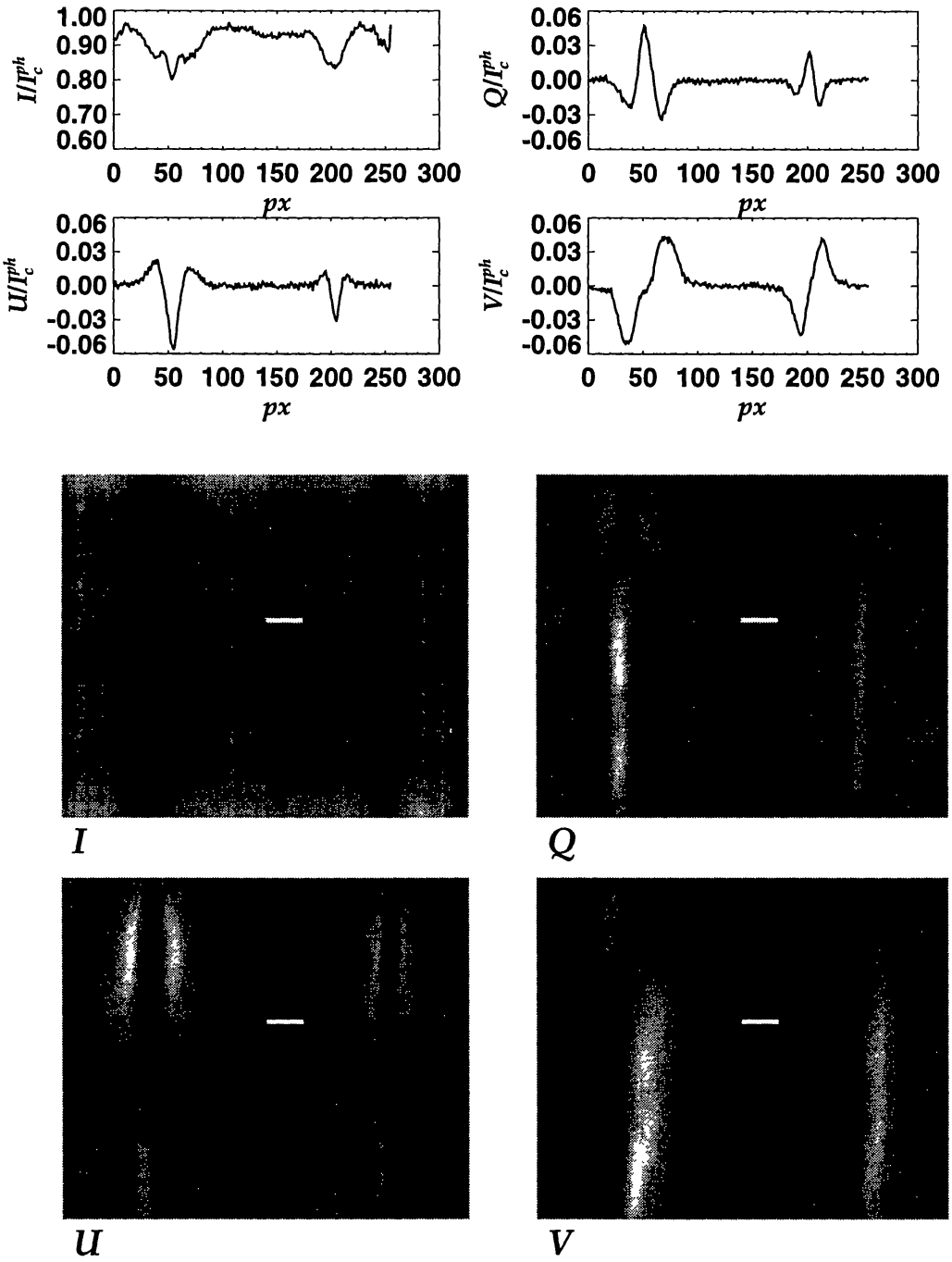


Figure 4. $I$, $Q$, $U$, and $V$ spectral images of a penumbral region taken with TIP in the region 1.5650 $\mu$m. The spectral range is about 7Å. The white line indicates the point on the slit for which the spectra are plotted

© Astronomical Society of the Pacific • Provided by the NASA Astrophysics Data System

1999ASPC..184....3C



$$\vec{\varepsilon} = (0.97, 0.61, 0.47, 0.51) \tag{48}$$

and

$$\sqrt{\varepsilon_2^2 + \varepsilon_3^2 + \varepsilon_4^2} = 0.92. \tag{49}$$

The modulation matrix given by Eq. 47 not only takes into account the behavior of the FLCs and the polarizer. The calibration optics (consisting of a linear polarizer and a retarder, which can be independently rotated) is located as far as possible from the polarization analyzer and a system composed by seven mirrors, which are in-between, are also calibrated (see Fig. 3). Figure 4 shows $I$, $Q$, $U$ and $V$ spectral images obtained with TIP at the German VTT, with the slit crossing the penumbra of a sunspot. No correction for telescope polarization has been applied. The profiles correspond to the point on the slit marked with a white line in the spectral images.

## 4. Magnetic Calibration

Once accurate polarimetric data are obtained, these have to be converted to the corresponding magnetic field vectors $\vec{B}$ (and their stratification with depth in the solar atmosphere) which originates them. Several procedures, with different levels of complexity, have been devised in the past to do so, especially depending on the kind of data obtained. Rather usual is the evaluation of single wavelength magnetograms, in which case a reference model atmosphere must be adopted to transform the observed degree of polarization (generally only circular) into magnetic field strength (e.g. Title & Tarbell 1977). The magnetic field orientation can only be obtained if the four Stokes parameters are available. This calibration procedure suffers from the disadvantage that it ignores the important effects of other quantities (such as temperature, line-of-sight velocity, micro- and macroturbulent velocities, filling factor, etc) on the determination of $\vec{B}$. For this reason, magnetograms are very inaccurate and should be used with caution, only as a qualitative determination of magnetic field presence. Despite their restrictions, they have been very widely used because of their simplicity (e.g., Title et al. 1987, Shine et al. 1994).

Figure 5 shows some illustrative examples of the trade-offs among parameters which may result from this kind of measurements. In the upper panel, several profiles of the FeI line at $\lambda$5250.2 Å are plotted. They all have the same observed $V/I$ value at $\Delta\lambda = -80$ mÅ from line center (a typical position where magnetographic signals are taken, see, e.g, Cauzzi et al. 1993, Title et al. 1987). The solid line in the plot has been obtained using Solanki's (1986) plage model atmosphere. The other line profiles have been obtained after modifying by a constant value a given quantity (shown by the labels in the plot), and varying the magnetic field stratification by an adequate constant. In this simulated magnetographic signal, no difference in the magnetic field may be inferred from the different measurements, unless more spectral information is obtained. The central and bottom panels show the amount by which the magnetic field stratification of Solanki's plage model atmosphere must be varied, by a constant value, to produce the same $V/I$ signal at $\Delta\lambda = -80$ mÅ, to compensate the change

© Astronomical Society of the Pacific • Provided by the NASA Astrophysics Data System

1999ASPC..184....3C



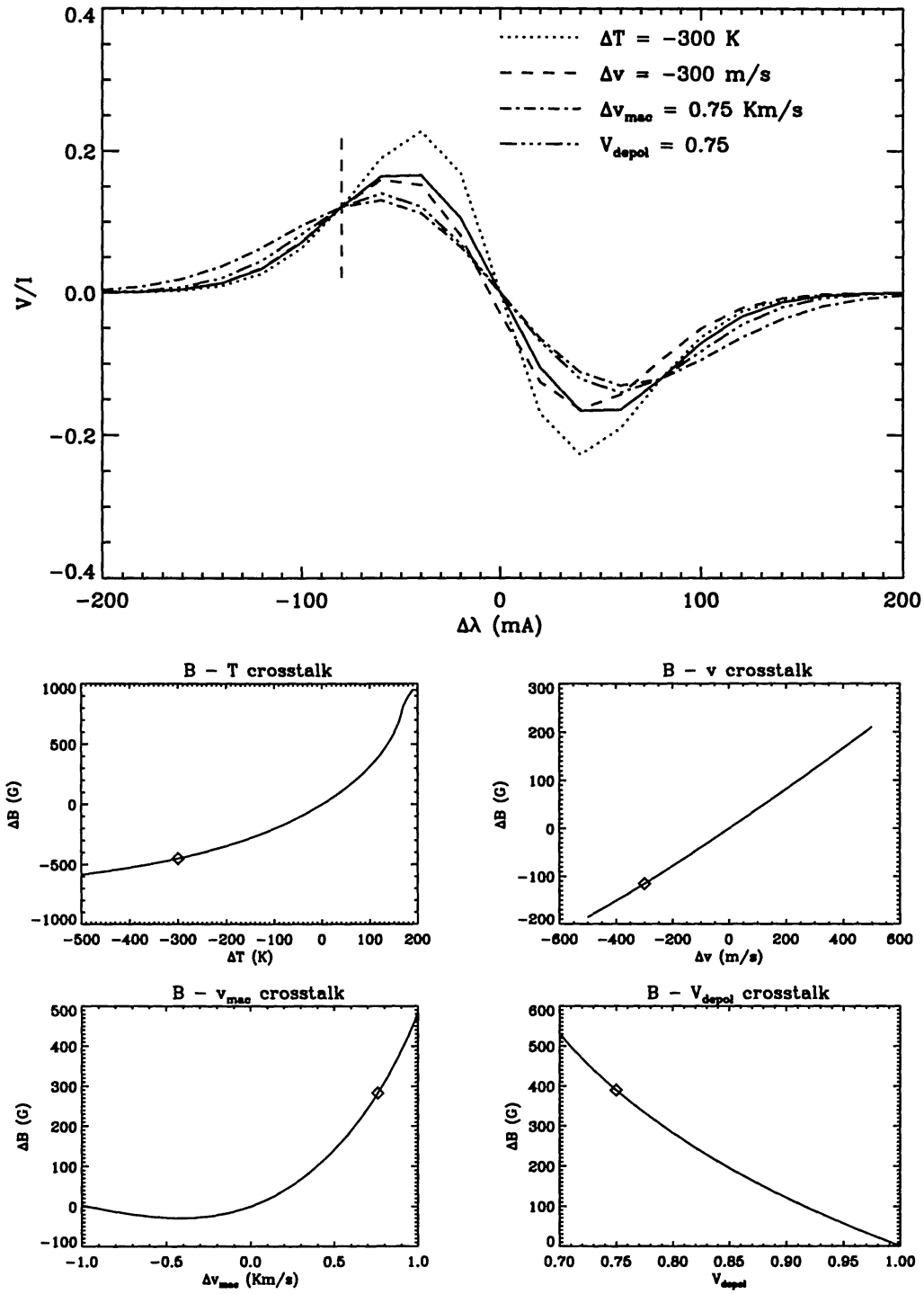


Figure 5. **Top**: Circular polarization ($V/I$) profiles obtained with different model atmospheres, giving rise to same value at $\Delta\lambda = -80$ mÅ from line center. **Center and bottom**: Crosstalk between magnetic field strength ($B$) and temperature ($T$), LOS velocity ($v$), macroturbulent velocity ($v_{\rm mac}$), and depolarization factor ($V_{\rm depol}$) (see text). The symbols correspond to the profiles shown in the upper panel.

© Astronomical Society of the Pacific • Provided by the NASA Astrophysics Data System

1999ASPC..184....3C



in a given individual parameter. In particular, the crosstalk of the magnetic field with temperature, line-of-sight velocity, macroturbulent velocity and depolarization factor is shown. As can be seen, magnetic fields derived from the calibration of magnetographic signals may be wrong by several hundreds Gauss. This uncertainty may be reduced if several wavelengths along the profiles are sampled. The conclusion is then reached that as much spectral information as possible is needed to avoid the crosstalk between the derived magnetic field and the other atmospheric quantities.

Several procedures which make use of more complete wavelength samplings or full line profiles have appeared in the literature. Among them, we may cite the center of gravity method (Rees & Semel 1979) or the weak field approximation (Landi Degl'Innocenti & Landi Degl'Innocenti 1973). More recently, Skumanich & Lites (1987) fitted full line profiles obtained with the ASP (with the FeI lines at $\lambda\lambda$ 6301.5 Å and 6301.5 Å) to those emerging from a Milne-Eddington atmosphere. A more sophisticated inversion scheme (called SIR, Stokes Inversion based on Response functions) was developed by Ruiz Cobo & del Toro Iniesta (1992). This code exploits the full diagnostic content of polarization profiles by first analyzing how the emergent spectra respond to perturbations of the atmospheric parameters (Ruiz Cobo & del Toro Iniesta 1994) and can handle arbitrary stratifications with depth of the relevant physical quantities. As a result, the shape of several spectral lines can be fitted within the noise of the measurements. The crucial point here is that all parameters are considered and modified simultaneously in order to assure self-consistency. The relevance of this approach for a precise and reliable determination of the atmospheric structure has been addressed in detail by del Toro Iniesta & Ruiz Cobo (1996). SIR has been successfully applied to a number of different solar observations (Collados et al. 1994, Bellot Rubio et al. 1997, 1999a, 1999b, Ruiz Cobo et al. 1997). As an illustrative example, Westendorp Plaza et al. (1997) have recently detected an Evershed flow returning to the photosphere, using ASP data and the SIR code. Comparisons of the ability of different methods to determine the magnetic field properties have been carried out by various authors (e.g., Cauzzi et al. 1993, Lites et al. 1994, Westendorp Plaza et al. 1998).

## 5. Physical Modeling

Despite the large advance represented by the inversion techniques for the interpretation of the measured polarimetric data, one must be very careful when applying them, indiscriminately, to any kind of observations. The analysis of polarization spectra requires a prior knowledge of the structures in which they originate because the observed profiles are invariably compared to spectral synthesis calculations that use prescribed scenarios. In this regard, we have to realize that any inversion of Stokes spectra is always model-dependent. For this reason, a careful selection of a suitable physical model is mandatory.

As in the case of the interpretation of magnetographic signals, where the selection of an adequate reference calibration model atmosphere plays a key role to obtain accurate magnetic determinations, the choice of a physical model to describe a given solar structure is also important to understand its properties and nature, especially when dealing with unresolved features. Some examples

© Astronomical Society of the Pacific • Provided by the NASA Astrophysics Data System

1999ASPC..184....3C



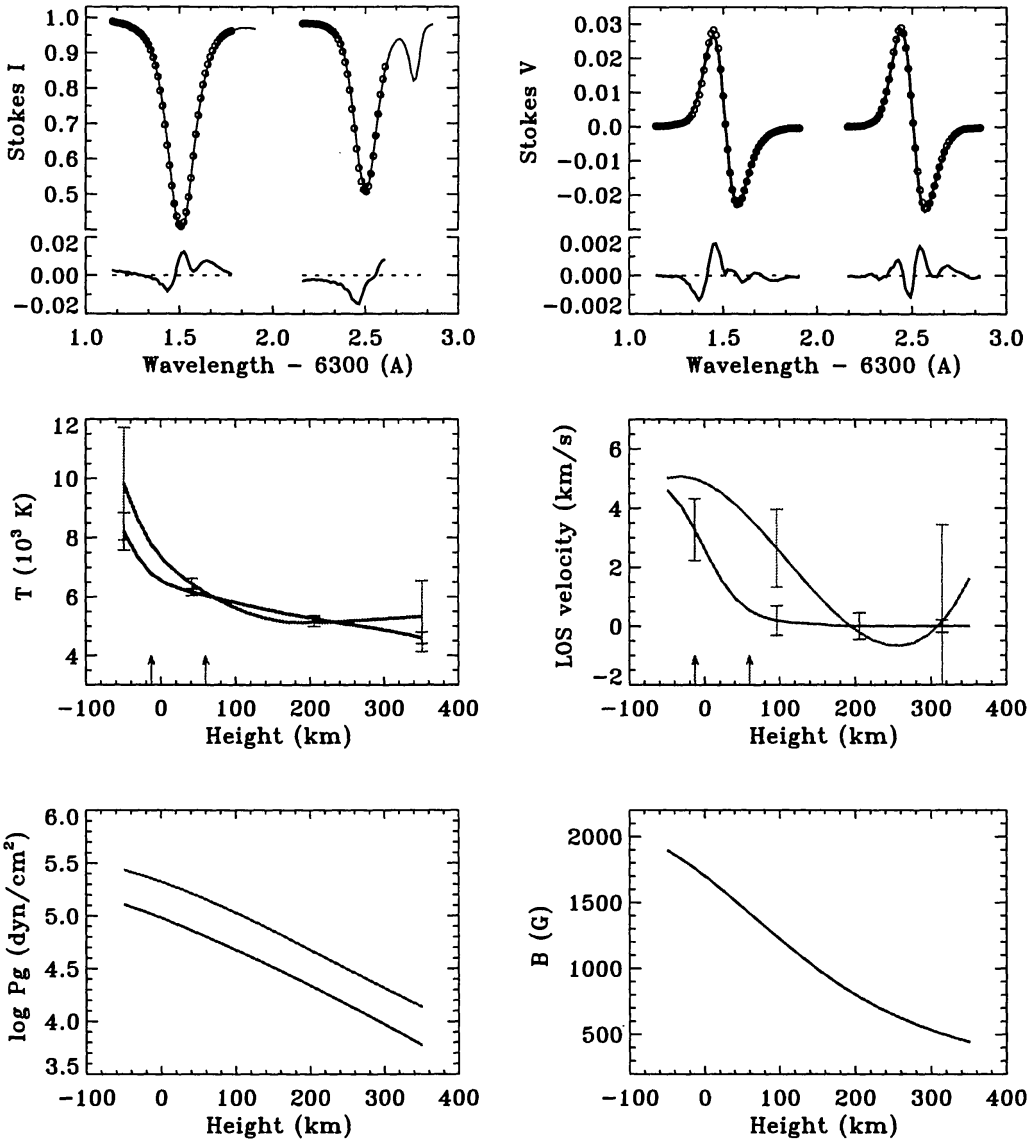


Figure 6. **Top**: Fit to $I$ and $V$ ASP observed profiles using the model by Bellot Rubio et al. (1999a). The circles indicate the observations and the solid line corresponds to the fits. Below are represented the residual errors. **Center and bottom:** External (black line) and internal (gray line) model atmospheres derived from the fits.

© Astronomical Society of the Pacific • Provided by the NASA Astrophysics Data System

1999ASPC..184....3C



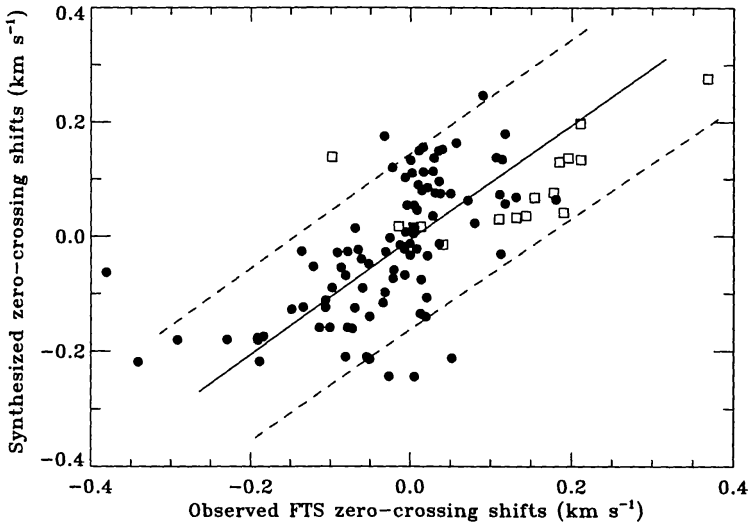


Figure 7. Comparison of observed and computed zero-crossing wavelengths by Bellot Rubio et al. (1999a) for 92 FeI lines (circles) and 16 FeII lines (squares). The solid line has a slope equal to unity. The dotted lines indicate the uncertainty of the FeI laboratory wavelengths.

might be quoted. In the following, different approaches to study the observed polarization signal coming from facular magnetic elements are presented as a particular example.

It is commonly accepted that subarcsecond magnetic structures exist on the solar surface and that they are not resolved by standard spectropolarimetric means. With this in mind, Bellot Rubio et al. (1997, 1999b) extended the original inversion code of Ruiz Cobo & del Toro Iniesta (1992) to deal with solar magnetic elements. The significant challenge of that code is the simultaneous inference, within the thin flux tube scenario, of the whole set of physical parameters considered relevant for the problem. These include the stratification with depth of temperature, magnetic field strength and LOS velocity. In this problem, the number of unknowns increases since the resolution element covers the magnetic atmosphere and the surrounding non-magnetic atmosphere. Hydrostatic equilibrium, horizontal pressure balance and magnetic flux conservation are used to impose reasonable constraints on the physical quantities of interest. The code has been successfully applied to ASP data of the FeI lines at $\lambda\lambda$ 6301.5 and 6302.5, recovering the full shape of $I$ and $V$ profiles within the noise (see Fig. 6). One of the most relevant results of this analysis is the need of strong downflows inside the flux tubes themselves. Frutiger and Solanki (1998) make another interpretation based on the same thin flux tube approximation, though.

An example of a completely different scenario which tries to explain the nature of facular and network magnetic fields are the MIcroStructured Magnetic Atmospheres (MISMA) proposed by Sánchez Almeida et al. (1996). Here, the relevant physical parameters fluctuate over scales much smaller than the typical photon mean free paths. Thus a MISMA model is, by definition, an inhomogeneous medium, where distinct atmospheres coexist. As shown by Sánchez

© Astronomical Society of the Pacific • Provided by the NASA Astrophysics Data System

1999ASPC..184....3C



Almeida (1997), observed polarization spectral line profiles in faculae and photospheric network can be very well reproduced in terms of MISMAs.

Since various approaches may give similar results in what concerns the quality of the fits to line profiles, the adequacy of the retrieved models can only be determined by their ability in reproducing observations other than those strictly used to obtain the free parameters of the models. In this regard, Bellot Rubio et al. (1997, 1999a) have demonstrated that their scenario (resulting from the inversion of only two spectral lines) is capable of matching the observed Stokes $V$ zero-crossing wavelengths of nearly one hundred FeI lines and sixteen FeII lines (see Fig. 7). Undoubtedly, it is through this kind of predictions that the realism of the different physical models may be put in evidence. This kind of tests together with the fast development of numerical simulations (see, e.g. Steiner et al. 1998) will finally give us the clue to understand the properties of small scale solar magnetic fields.

**Acknowledgments.** Thanks are due to L.R. Bellot Rubio and B. Ruiz Cobo for modifying the inversion code to deal with magnetographic signals and for help and discussion during the elaboration of the manuscript. This work has been funded by the Spanish DGES under project 95-0028.

## References

Balasubramaniam, K.S., Venkatakrishnan, P., & Bhattachariyya, J.C. 1985, Solar Phys., 99, 333

Ballesteros, E., Collados, M., Bonet, J.A., et al. 1996, A&AS, 115, 353

Bellot Rubio, L.R., Ruiz Cobo, B., & Collados, M. 1997, ApJ, 478, L45

Bellot Rubio, L.R., Ruiz Cobo, B., & Collados, M. 1999a, A&A, 341, L31

Bellot Rubio, L.R., Ruiz Cobo, B., & Collados, M. 1999b, ApJ(submitted)

Capitani, C., Cavallini, F., Ceppatelli, G., et al. 1989, Solar Phys., 120, 173

Cauzzi, G., Smaldone, L.A., Balasubramaniam, K.S., & Keil S.L. 1993, Solar Phys., 146, 207

Collados, M., Martínez Pillet, V., Ruiz Cobo, B., del Toro Iniesta, J.C., Vázquez, M. 1994, A&A, 291, 622

Elmore, D.F., Lites, B.W., Tomczyk, S., et al. 1992 SPIE Proceedings, 1746, 22

Fried, D.L. 1965, J. Opt. Soc. American, 55, 1427

Frutiger, C., Solanki, S.K. 1998 A&A, 336, L65

Keller, C.U., Deubner, F.L, Egger, U., Fleck B., & Povel H.P. 1994, A&A, 286, 626

Landi Degl'Innocenti, E., & Landi Degl'Innocenti, M. 1973, Solar Phys. 31, 299

Lide, D.R. 1993, CRC Handbook of Chemistry and Physics

Lites, B.W., Martínez Pillet, V., & Skumanich A. 1994, Solar Phys. 155, 1

Martínez Pillet, V. 1997, in 1st ASPE meeting: Advances in the Physics of Sunspots, (eds.) Schmieder, B., del Toro Iniesta, J.C., & Vázquez, M., A.S.P. Conf. Series, 118, 212

Martínez Pillet, V., Collados, M., Sánchez Almeida, J. et al. 1999, in High Resolution Solar Physics: Theory Observations and Techniques, 19th

© Astronomical Society of the Pacific • Provided by the NASA Astrophysics Data System

1999ASPC..184....3C



NSO/Sacramento Peak Summer Workshop, (eds.) Rimmele T., & Balasubramaniam K.S. (in press)

Parker, E.N. 1978, ApJ, 221, 368

Press, W.H., Flannery, B.P., Teukolsky, S.A., & Vetterling, W.T. 1986, Numerical Recipes, Cambridge Univ. Press.

Rees D.E., & Semel M.D. 1979, A&A, 74, 1

Ruiz Cobo, B., Rodríguez Hidalgo, I., & Collados, M. 1997, ApJ, 488, 462

Ruiz Cobo, B., & del Toro Iniesta, J.C. 1992, ApJ, 398, 375

Ruiz Cobo, B., & del Toro Iniesta, J.C. 1994, A&A, 283, 129

Sánchez Almeida, J., & Martínez Pillet, V. 1994, ApJ, 424, 1014

Sánchez Almeida, J., Collados, M., & Martínez Pillet V. 1994, Modulation Schemes for the Polarimeter of the SVST, IAC internal report

Sánchez Almeida, J., Landi Degl'Innocenti, E., Martínez Pillet, V, & Lites, B.W. 1996, ApJ, 466, 537

Sánchez Almeida, J. 1997, ApJ, 491, 993

Shine, R.A., Title, A.M., Tarbell, T.D., Smith, K., & Frank Z.A. 1994, ApJ, 430, 413

Skumanich, A., & Lites B.W. 1987, ApJ, 322, 473

Solanki, S.K. 1986, A&A, 168, 311

Steiner, O., Grossmann-Doerth, U., Knölker, M., & Schüssler, M. 1998, ApJ, 495, 468

Stenflo, J.O., & Povel H.P. 1985, Appl.Optics, 24, 3893

Stenflo, J.O., Keller, C.U., & Povel H.P. 1992, LEST Technical Report No. 54.

Title, A.M., & Tarbell, T.D. 1977. Solar Phys., 52, 113

Title, A.M., Tarbell, T.D., & Topka, K.P. 1987, ApJ, 317, 892

del Toro Iniesta, J.C., & Ruiz Cobo, B. 1996, Solar Physics, 164, 169

Westendorp Plaza, C., del Toro Iniesta, J.C., Ruiz Cobo, B., Martínez Pillet, V., Lites, B.W., & Skumanich, A. 1997, Nature, 389, 47

Westendorp Plaza, C., del Toro Iniesta, J.C., Ruiz Cobo, B., Martínez Pillet, V., Lites, B.W., & Skumanich, A. 1998, ApJ, 494, 453

© Astronomical Society of the Pacific • Provided by the NASA Astrophysics Data System